COMPARATIVE ANALYSIS OF TiO_2 NANOTUBE LAYERS FORMED BY SINGLE- AND TWO-STEP ANODIZATION: SURFACE MORPHOLOGY, CORROSION RESISTANCE, AND CELLULAR RESPONSE

Van Toan Le[1,2], Minh Duc Dang[1], Cong Manh Vu[1], Hung Vuong Pham[1,3,*]

[1]*School of Materials Science and Engineering, Hanoi University of Science and Technology*

[2]*Faculty of Physics and Chemical Engineering, Le Quy Don Technical University*

[3]*Laboratory of Biomedical Materials, Hanoi University of Science and Technology*

Abstract

This study examines the influence of anodization procedures on the formation and properties of TiO_2 nanotube layers on commercially pure titanium (cp-Ti) for biomedical implant applications. Both single-step (TiO_2 1S) and two-step (TiO_2 2S) anodization produced nanotubular structures composed of anatase and rutile phases, with the two-step process yielding more uniform and vertically aligned nanotubes. Mechanical testing indicated an increase in surface hardness, while electrochemical analyses demonstrated enhanced corrosion resistance, particularly for the TiO_2 2S sample. Furthermore, TiO_2 2S surfaces promoted superior cell adhesion and spreading, with well-developed filopodia and lamellipodia. Overall, the two-step anodization produces a more stable, oxygen-rich oxide layer with improved durability and biocompatibility, highlighting its potential for bone implant applications.

Keywords: *Titanium; TiO_2 nanotubes; anodization; surface modification; corrosion resistance; cell adhesion; biomedical implants.*

1. Introduction

Titanium and its alloys have long been considered ideal materials for biomedical implants due to their excellent biocompatibility, high mechanical strength, and superior corrosion resistance [1]-[4]. However, in their native state, titanium surfaces are often biologically inert, limiting their ability to effectively integrate with surrounding bone tissue and potentially compromising the long-term success of implants [5].

To overcome this limitation, various surface modification techniques have been developed to enhance biological performance [6]-[8]. Among these, electrochemical anodization has emerged as a simple and controllable method capable of producing self-organized TiO_2 nanotube arrays on titanium substrates [9]-[11]. These nanotubular structures not only increase surface area and roughness but also provide microscale

* Corresponding author, email: vuong.phamhung@hust.edu.vn

DOI: 10.56651/lqdtu.jst.v3.n02.1052.pce

topographical cues that promote cell adhesion, proliferation, and osteogenic differentiation [12]-[14].

The morphology, size, and orientation of TiO_2 nanotubes are strongly influenced by anodization parameters, including applied voltage, electrolyte composition, and processing time [15]-[17]. Multi-step anodization strategies, particularly those involving stepwise voltage control, have been proposed to improve the uniformity and vertical alignment of nanotube architectures compared to conventional single-step methods [18]-[21]. Despite this potential, there is a lack of systematic comparisons between single-step and two-step anodization approaches under identical processing conditions, especially on commercially pure titanium (cp-Ti), which is widely used in orthopedic and dental applications [22].

This study aims to evaluate the effects of single-step and two-step anodization processes on the formation of TiO_2 nanotube layers on cp-Ti substrates. Comprehensive analyses were conducted to assess surface morphology, chemical composition, crystalline structure, corrosion resistance, and invitro cell adhesion. The objective is to optimize voltage-controlled anodization as a practical strategy to enhance the biological performance of titanium implants in orthopedic applications.

2. Experiment

2.1. Anodization of titanium

Commercially pure titanium (Grade 2) plates with dimensions of 10 × 10 × 1 mm were mechanically polished using silicon carbide (SiC) abrasive papers of increasing grit size, followed by ultrasonic cleaning in ethanol and deionized water to remove surface contaminants. Anodization was performed using an electrolyte composed of 0.5 wt% ammonium fluoride (NH_4F) and 2 vol% deionized water dissolved in 50 mL of ethylene glycol. All reagents were obtained from Sigma-Aldrich.

The two-step anodization process was conducted as follows: in the first step, samples were anodized at 25 V for 25 minutes at room temperature. After rinsing and gently removing the initial oxide layer, a second anodization was carried out at 50 V for 45 minutes under the same conditions to promote the formation of a more ordered TiO_2 nanotube structure. The anodized specimens were then thoroughly rinsed with deionized water and dried using hot air.

For comparison, a control group was anodized using a single-step process (designated as TiO_2 1S) at 50 V for 60 minutes at room temperature, to evaluate the differences between one-step and two-step anodization treatments.

2.2. Surface morphology and structural characterization

The morphology of the anodized titanium surfaces was examined using scanning electron microscopy (SEM) to evaluate the diameter, alignment, and surface coverage of the TiO_2 nanotubes. Structural analysis was conducted by X-ray diffraction (XRD) using a Kα diffractometer operating at 30 kV, with measurements taken in the 2θ range of 20° to 80° to identify crystalline phases. The elemental composition and distribution on the sample surfaces were further analyzed using energy-dispersive X-ray spectroscopy (EDX) integrated with the SEM system.

2.3. Electrochemical corrosion assessment

The corrosion resistance of the anodized titanium was evaluated in simulated body fluid (SBF) maintained at 37 ± 0.5°C. Tafel polarization was performed with a scanning range of ±100 mV relative to the open circuit potential (OCP) to determine the corrosion potential (E_{corr}) and corrosion current density (I_{corr}). The anodic Tafel slope (α) was obtained from the polarization curves, and the polarization resistance (R_p) as well as the protection efficiency (PE) were calculated accordingly.

Electrochemical impedance spectroscopy (EIS) was conducted over a frequency range from 10^5 Hz to 100 mHz, with a sinusoidal perturbation amplitude of 100 mV. Equivalent circuit fitting provided the solution resistance (R_s), oxide layer resistance (R_n), and a constant phase element (CPE), characterized by its magnitude (Y_o) and exponent (n), which describe the non-ideal capacitive behavior of the oxide layer. In the case of anodized samples, a Warburg element (W) was additionally used to represent ion diffusion through the nanotube structures.

All electrochemical tests were conducted using a conventional three-electrode system, with the anodized titanium as the working electrode, a silver/silver chloride (Ag/AgCl) electrode as the reference, and a platinum plate as the counter electrode.

2.4. Preliminary biocompatibility evaluation

The biocompatibility of the anodized surfaces was assessed in vitro using baby hamster kidney (BHK) fibroblast cells. Prior to cell culture, the samples were sterilized using a dry autoclave method at 160°C for 2 hours. Cells were seeded directly onto the sample surfaces and incubated for 72 hours in standard cell culture conditions (37°C, 5% CO_2, 95% relative humidity). After incubation, the samples were fixed and dehydrated in a graded ethanol series before being dried and sputter-coated with gold. Cell attachment and morphology on the material surface were observed using a mini-SEM to provide initial insight into the interaction between cells and the nanotube-modified titanium surfaces.

3. Results and discussion

3.1. X-ray diffraction (XRD) patterns

The X-ray diffraction (XRD) patterns of the three specimens (Fig. 1) exhibit distinct differences in crystalline phases following anodization treatments. The untreated titanium (Ti) sample displays diffraction peaks at 2θ positions corresponding to the (100), (002), (101), (102), (110), (103), (112), and (201) planes, consistent with the standard reference card for titanium (PDF 44-1294) [22]. This confirms that the base material possesses a typical hexagonal close-packed (hcp) crystal structure of commercial titanium, with no significant presence of oxide phases, indicating that the native oxide layer is extremely thin and below the XRD detection limit.

After single-step anodization, the TiO_2 1S sample exhibits additional peaks at positions corresponding to the (101), (004), (200), (105), (211), (116), (215), and (103) planes, matching the anatase phase according to PDF 21-1272 [23]-[25]. A minor peak near 27.4°, corresponding to the (110) plane of rutile (PDF 21-1276) [26], [27], is also detected, indicating a small fraction of rutile. These results confirm the formation of a TiO_2 oxide layer predominantly composed of anatase, with minor rutile content. The persistence of some titanium substrate peaks suggests that the oxide layer is not yet thick enough to fully mask the underlying metal.

In contrast, the TiO_2 2S sample exhibits sharper and more intense anatase peaks, particularly at the characteristic planes (101), (004), (200), (105), (211), (116), (215), and (103). The rutile signals are negligible, indicating that the two-step anodization promotes the formation of an anatase-dominant oxide layer with higher TiO_2 content. The increased diffraction intensity is attributed to the thicker oxide film and the porous nanotubular structure rather than an increase in crystallinity. As the nanotube layer becomes more porous, the diffraction signals sharpen, and the titanium substrate peaks are more pronounced compared with the TiO_2 1S sample.

These results confirm that both anodization treatments generate TiO_2 layers on the titanium surface. Compared with single-step anodization, the two-step process improves the coverage and relative contribution of the TiO_2 phase, with anatase remaining dominant. Such enhancements in oxide layer thickness and composition contribute to the improved corrosion resistance and biocompatibility of the anodized materials.

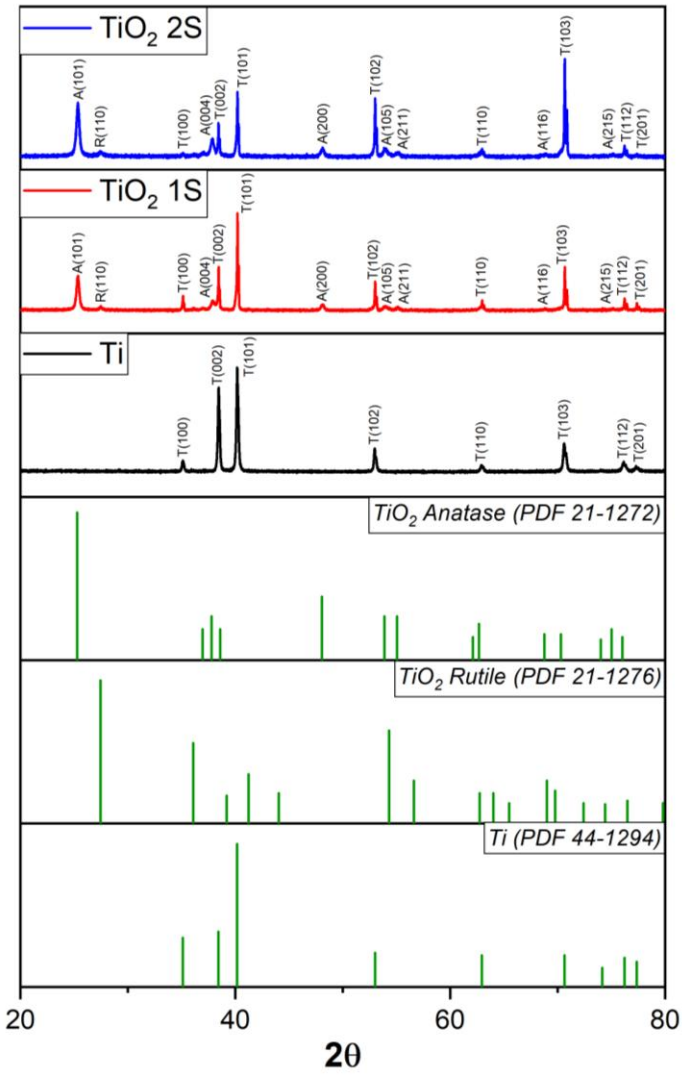

Fig. 1. X-ray diffraction patterns of the samples compared with standard reference cards (T: titanium, A: anatase, R: rutile).

3.2. Surface morphology

The SEM image at 2000X magnification (Fig. 2) reveals the mechanically treated titanium surface, characterized by elongated scratches aligned in a single direction, typical of grinding or polishing processes. The surface appears relatively smooth, with no apparent microstructural features or surface modifications associated with chemical treatment.

Such a surface structure is generally unfavorable for cell adhesion and biological interactions due to the lack of anchoring points and limited surface area. Therefore, this untreated titanium substrate serves as a baseline reference for comparison with surface-modified samples, allowing for the evaluation of improvements in both biological and mechanical performance.

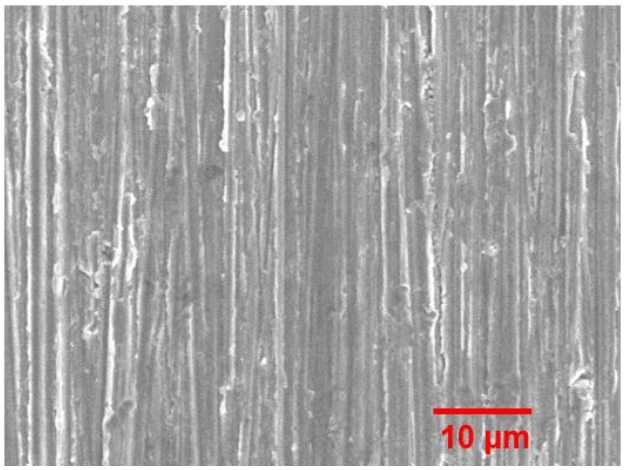

Fig. 2. Surface morphology of mechanically treated titanium substrate.

SEM images at 20000X magnification (Fig. 3) reveal the morphology of the TiO_2 layers obtained from single-step (Fig. 3a) and two-step (Fig. 3b) anodization.

For the TiO_2 1S sample (Fig. 3a), a well-defined nanotubular structure is observed, with uniformly distributed, circular pore openings and consistent tube diameters. In some areas, crystalline oxide features can be seen along the tube walls, although the overall structure remains open and vertically oriented. This morphology is characteristic of a stable oxide layer formed under optimized single-step anodization conditions.

In contrast, the TiO_2 2S sample (Fig. 3b) exhibits a rougher and more porous surface, with smaller, densely packed nanotubes whose individual openings are less distinguishable. This may reflect slight dissolution or structural reorganization during the second anodization step, resulting in a more homogeneous but less oriented surface. However, the increased nanoporous density may contribute positively to biological interactions by enhancing protein adsorption and cellular attachment.

Both samples successfully developed nanostructured TiO_2 layers, with the two-step anodized surface exhibiting higher porosity and tube density, which may be advantageous for biomedical applications.

SEM images at 50000X magnification (Fig. 4) provide a more detailed view of the TiO_2 nanotube structures formed after single-step (Fig. 3a) and two-step (Fig. 3b) anodization.

In the TiO_2 1S sample (Fig. 4a), the nanotube array is well-defined, with uniformly distributed circular openings and nearly identical diameters. The nanotube layer displays a high degree of order, typical of stable oxide growth under well-controlled anodization conditions. Thin, plate-like crystalline oxide features observed along some tube walls may result from post-treatment crystallization or residual salts from the electrolyte.

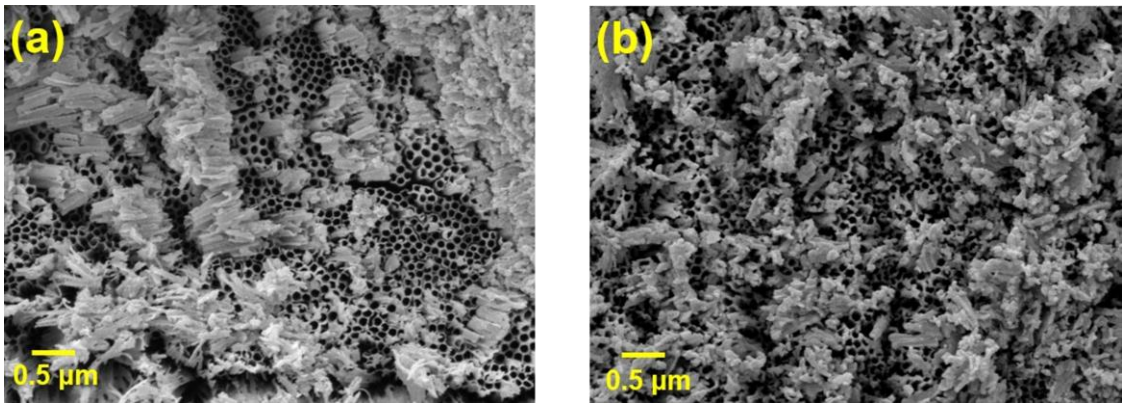

Fig. 3. Surface morphology of anodized titanium:
(a) TiO_2 1S and (b) TiO_2 2S, observed at 20000X magnification.

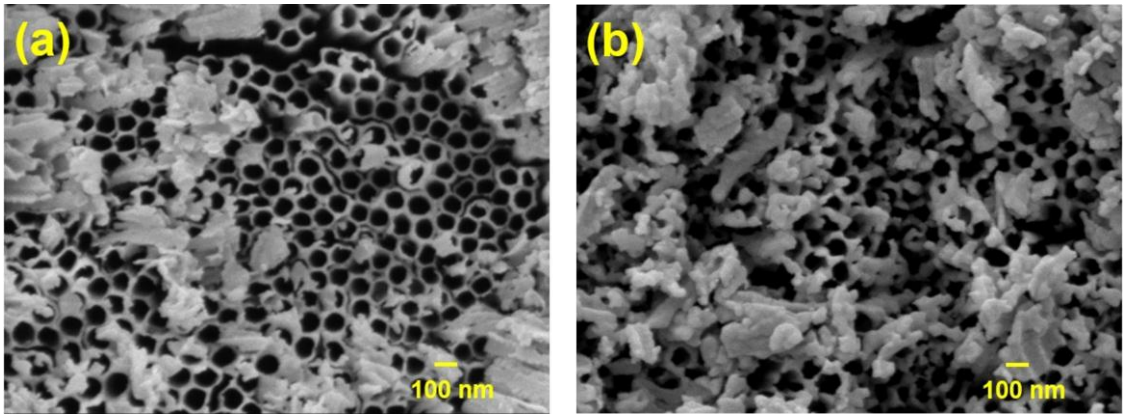

Fig. 4. Surface morphology of anodized titanium:
(a) TiO_2 1S and (b) TiO_2 2S, observed at 50000X magnification.

In contrast, the TiO_2 2S sample (Fig. 4b) still exhibits a nanotubular morphology, but the pore openings appear less uniform and less clearly defined compared to the 1S sample. The surface appears more porous, with numerous crystalline structures partially covering the tube mouths, giving rise to a rougher texture. These changes are likely associated with the second anodization step, which may induce localized dissolution or structural rearrangement of the oxide layer, leading to increased microstructural density but reduced order in the nanotube array.

At higher magnification, both samples maintain a nanotubular architecture; however, the TiO_2 2S surface demonstrates greater porosity and structural density, whereas the TiO_2 1S nanotube layer presents a more uniform and well-defined morphology. These morphological differences may directly influence protein adsorption, cell adhesion, and the overall biological integration of the implant surface [28], [29].

3.3. Surface chemical composition

The EDX spectra presented in Fig. 5 illustrate the surface elemental composition of the TiO_2 layers formed by single-step and two-step anodization.

For the TiO_2 1S sample (Fig. 5a), the EDX spectrum revealed atomic percentages of 56.4% Ti, 35.5% O, and 9.1% F. In contrast, the TiO_2 2S sample (Fig. 5b) showed a lower Ti content (50.8%), a higher O content (39.7%), and a comparable F content (9.5%). The reduction in titanium accompanied by the increase in oxygen clearly reflects a higher oxidation degree in the 2S sample, which is consistent with the formation of a thicker and more developed oxide film during the two-step anodization process [20].

The similar fluorine content in both samples confirms that F^- ions from the NH_4F electrolyte were incorporated into the oxide layer regardless of the anodization procedure. Overall, the comparison between Fig. 5a and Fig. 5b demonstrates that the two-step anodization yields a TiO_2 layer richer in oxygen and with a more complete oxide structure than the single-step anodization, in agreement with the morphological and electrochemical observations discussed above.

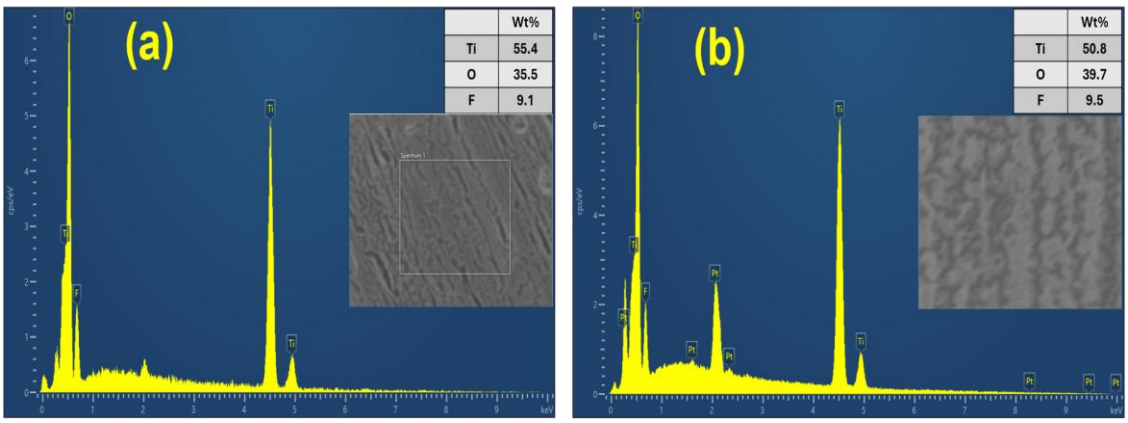

Fig. 5. EDX spectra of anodized surfaces (a) TiO_2 1S and (b) TiO_2 2S.

3.4. Mechanical properties evaluation

The Vickers hardness values of titanium, TiO_2 1S, and TiO_2 2S are presented in Tab. 1 to evaluate the effect of the TiO_2 oxide layer on the surface mechanical properties. The results clearly indicate an improvement in hardness after anodization, particularly in the two-step treated sample.

Tab. 1. Hardness of titanium before and after anodization

Samples	Measurement 1 (HV)	Measurement 2 (HV)	Measurement 3 (HV)	Average (HV)
Ti	139	133	131	132.67 ± 1.20
TiO_2 1S	138	142	146	142.67 ± 2.03
TiO_2 2S	143	148	139	143.33 ± 3.68

The hardness measurements indicate that both anodized samples (TiO_2 1S and TiO_2 2S) exhibited higher average hardness values compared to the untreated Ti sample. The Ti sample showed the lowest hardness, with an average value of 132.67 ± 1.20 HV, reflecting the intrinsic mechanical properties of the as-received titanium substrate.

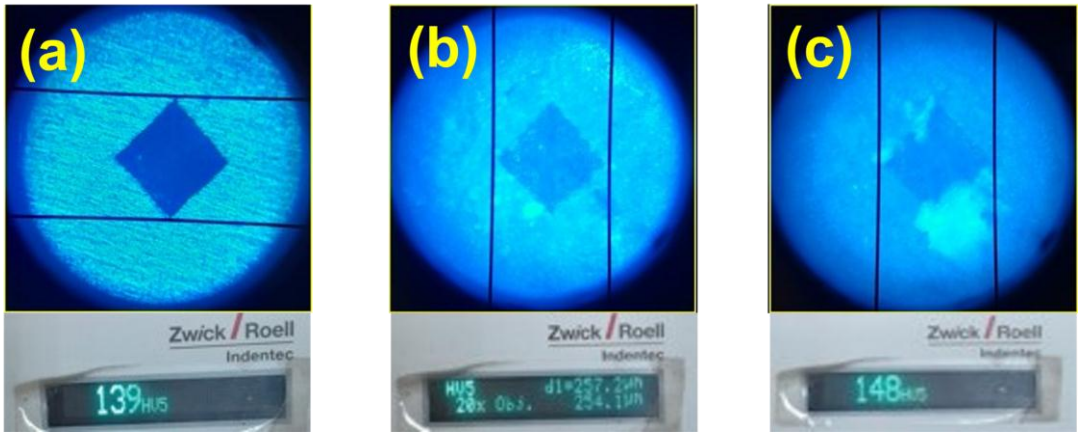

Fig. 6. Hardness indents on (a) Ti, (b) TiO_2 1S, and (c) TiO_2 2S.

Following single-step anodization, the TiO_2 1S sample exhibited a significant increase in hardness, reaching an average value of 142.67 ± 2.03 HV. This enhancement can be attributed to the formation of a thick and hard TiO_2 oxide layer, which improves resistance to localized plastic deformation under applied load.

The TiO_2 2S sample showed the highest hardness, averaging 143.33 ± 3.68 HV. The oxide layer formed via the two-step process may have a more uniform and well-crystallized structure, contributing to superior mechanical reinforcement. Although the standard deviation for the 2S sample was slightly higher, the difference compared to the 1S sample remained within an acceptable range, indicating good consistency in mechanical performance.

These results suggest that anodization not only enhances the biological properties but also improves the surface mechanical characteristics of titanium. Among the tested samples, TiO_2 2S demonstrated the most promising overall performance, making it a potential candidate for applications requiring both high surface hardness and enhanced

biocompatibility [30]. Representative marks obtained during the hardness measurements are shown in Fig. 6.

3.5. Current response and oxide formation behavior

The current–time (I–t) curves in Fig. 7 reveal clear differences in oxide formation behavior between the two anodization modes.

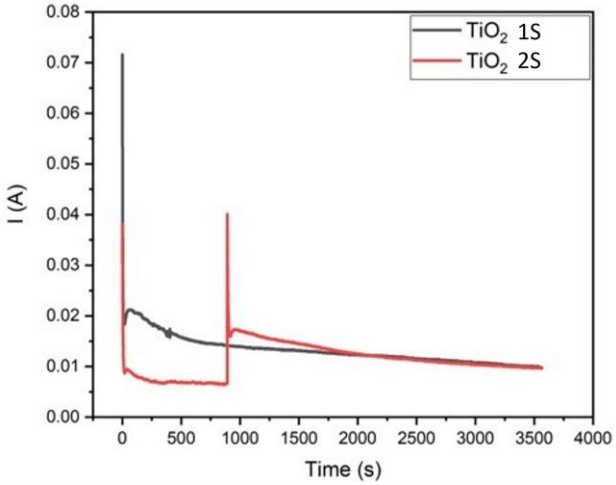

Fig. 7. Current–time (I–t) curves of the TiO_2 1S and TiO_2 2S anodization processes.

For the TiO_2 1S sample, the current decreases rapidly and reaches a steady state early, indicating uniform and consistent oxide layer formation. In contrast, the TiO_2 2S sample exhibits two distinct current phases: an initial decline followed by a noticeable increase at the transition point between the two steps. This rise suggests re-initiation of oxide growth associated with the second anodization stage.

These results indicate that the two-step anodization process promotes a more dynamic and extended oxide growth process, likely resulting in a thicker and more porous TiO_2 layer, as corroborated by SEM observations.

3.6. Electrochemical properties

The Tafel polarization curves in Fig. 8, together with the electrochemical parameters summarized in Tab. 1, demonstrate a significant improvement in the corrosion resistance of titanium following anodization.

The untreated titanium sample exhibited the highest corrosion current density (i_{corr}), reaching 3.63×10^{-6} A/cm², corresponding to a corrosion rate (CR) of 0.0421 mm/year. After anodization, the TiO_2 1S sample showed a reduced current density of 1.98×10^{-6} A/cm² with a corresponding corrosion rate of 0.0230 mm/year. The TiO_2 2S sample exhibited the lowest corrosion current density of 1.73×10^{-6} A/cm² and a corrosion rate of 0.0201 mm/year. In addition, the polarization resistance (R_p)

increased significantly from 13,803 to 33,188 and 33,131 Ω·cm² for the TiO_2 1S and TiO_2 2S samples, respectively, indicating the formation of a stable passive oxide layer that effectively enhances barrier properties against corrosive attack.

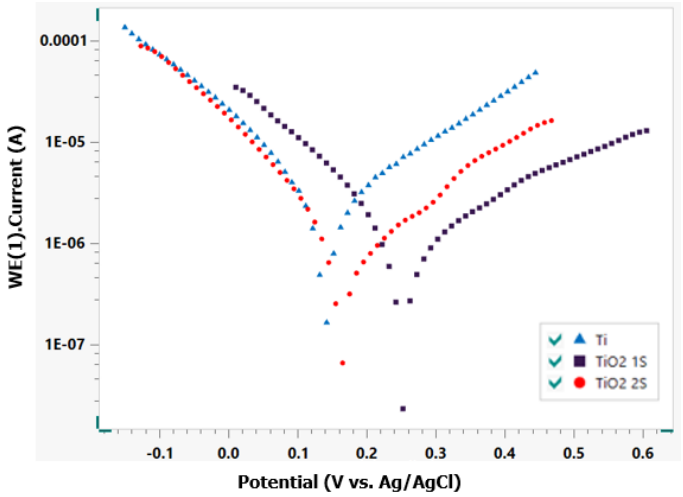

Fig. 8. Tafel polarization curves of titanium before and after anodization.

Comparison between the two surface treatments reveals that the TiO_2 2S sample provides better corrosion protection than the TiO_2 1S sample. The two-step sample exhibited a protection efficiency (PE) of 52.32%, notably higher than the 45.43% recorded for the single-step treatment (Tab. 2). This difference underscores the considerable influence of processing conditions on oxide layer quality and overall corrosion resistance.

Tab. 2. Corrosion parameters obtained from Tafel polarization curves for untreated and anodized titanium samples

Sample	**E_{corr} (V)**	**I_{corr} (A/cm²)**	**Corrosion rate (mm/year)**	**R_p (Ω·cm²)**	**PE (%)**
Ti	0.13981	3.63×10^{-6}	0.042137	13,803	0
TiO_2 1S	0.25106	1.98×10^{-6}	0.023017	33,188	45.43
TiO_2 2S	0.16302	1.73×10^{-6}	0.020083	33,131	52.32

Although the TiO_2 1S sample exhibited a more noble corrosion potential, its actual protective performance was inferior to that of the TiO_2 2S sample. This indicates that corrosion potential (E_{corr}) alone is not sufficient to fully assess protective efficiency; a comprehensive evaluation should also consider corrosion current density and polarization resistance for a more accurate conclusion.

Based on the electrochemical results, anodization proves to be an effective method for enhancing the corrosion resistance of titanium. The two-step process

demonstrated superior performance and holds strong potential for application in biomedical implants requiring long-term stability in physiological environments.

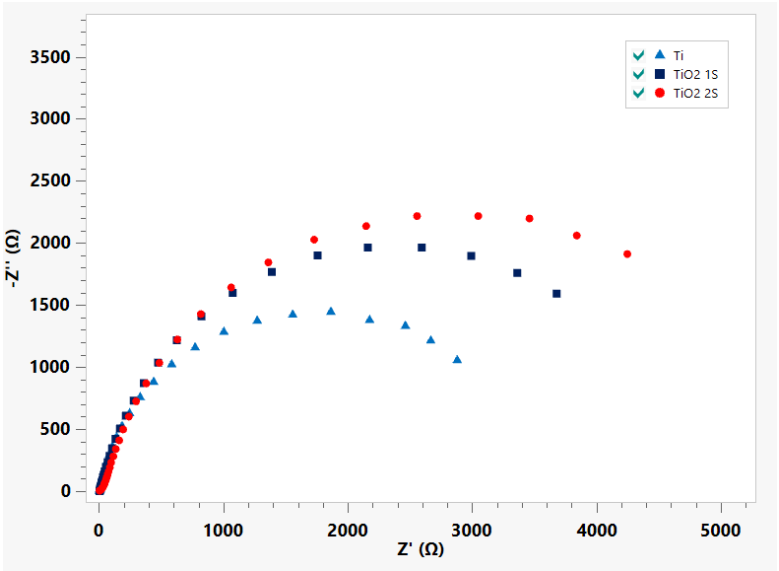

Fig. 9. Nyquist plots of titanium before and after anodization.

The Nyquist impedance spectrum in Fig. 9 clearly demonstrates the enhanced electrochemical behavior of the anodized samples. The untreated titanium (Ti) exhibited the smallest semicircular arc, ending around 3000 Ω on the Z' axis, corresponding to a charge transfer resistance (R_p) of 3.62 kΩ (Tab. 3). This indicates the presence of a thin, weakly protective native oxide layer.

Tab. 3. Electrochemical impedance parameters obtained from Nyquist plots of titanium before and after anodization

Sample	**R_s (Ω)**	**Y_0 (μS·s^n)**	**n**	**R_{ct} (kΩ)**	**σ (mΩ·s$^{-0.5}$)**
Ti	4.23	194	0.870	3.62	—
TiO_2 1S	3.99	143	1.060	3.06	925
TiO_2 2S	4.16	158	0.917	4.23	5.61

Figures 10 and 11 show the equivalent electrical circuits used to model the EIS response of titanium surfaces. In Fig. 10, R_n represents the polarization resistance of the native oxide, and CPE_n models its non-ideal capacitive behavior, while R_s is the solution resistance. In Fig. 11, R_a and CPE_a correspond to the anodized oxide layer, W represents Warburg impedance due to ion diffusion, and R_s is again the solution resistance. These circuits capture both charge transfer and diffusive processes in the respective oxide layers.

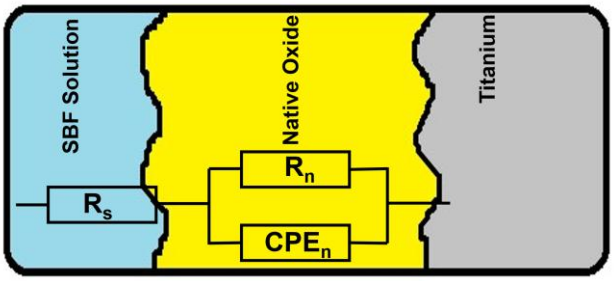

Fig. 10. Equivalent electrical circuit used to model the EIS response of untreated titanium.

The TiO_2 1S sample exhibited a relatively large Nyquist arc, although its charge transfer resistance (R_n = 3.06 kΩ) was slightly lower. The pronounced low-frequency tail and high Warburg coefficient (σ = 925 $m\Omega \cdot s^{-0.5}$) indicate substantial ion diffusion, likely arising from a porous or heterogeneous oxide structure.

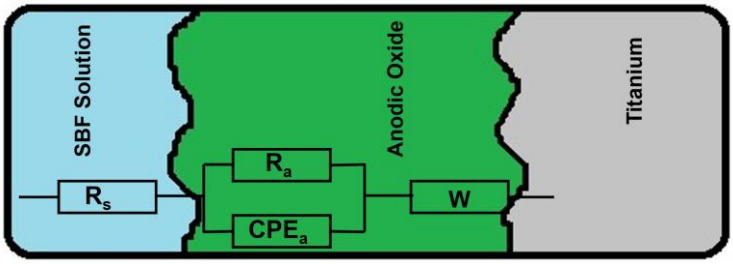

Fig. 11. Equivalent electrical circuit used to model the EIS response of anodized titanium.

In contrast, the TiO_2 2S sample displayed the largest Nyquist arc with the highest charge transfer resistance (R_a = 4.23 kΩ), and a gentler low-frequency slope, corresponding to a markedly lower Warburg coefficient (σ = 5.61 $m\Omega \cdot s^{-0.5}$). This suggests the formation of a denser, more compact oxide layer, which effectively hinders both charge transfer and ionic diffusion. The trends observed are consistent with the equivalent circuit models: while the bare Ti surface could be modeled using a simple Randles circuit, the anodized samples required an additional Warburg element to capture diffusion effects. Table 3 further highlights variations in CPE values and exponents nnn, reflecting differences in dielectric behavior and layer uniformity.

Overall, anodization improves charge transfer resistance and introduces diffusion impedance, with the two-step anodization producing a particularly stable oxide layer exhibiting superior corrosion resistance.

3.7. Evaluation of extract biocompatibility

The scanning electron microscopy (SEM) images after 48 hours of cell culture (Fig. 12) clearly demonstrate the differences in cell adhesion and spreading among the three samples.

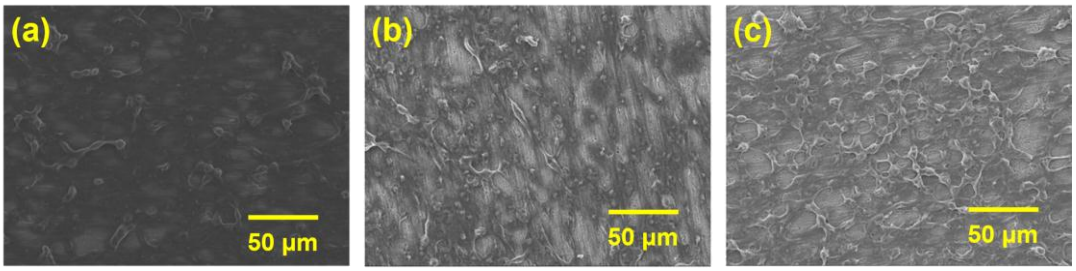

Fig. 12. SEM images showing BHK cell distribution after 48 hours of culture on (a) titanium, (b) TiO_2 1S, and (c) TiO_2 2S.

On the untreated titanium surface (Fig. 12a), cells appear sparsely distributed with predominantly rounded or slightly elongated morphologies, indicating limited adhesion. This suggests that the native titanium surface lacks favorable microstructural features and possesses low bioactivity, resulting in poor cell attachment.

For the TiO_2 1S sample (Fig. 12b), a higher cell density is observed, with cells exhibiting a more flattened morphology aligned along the surface topography. This reflects the role of the anodized oxide layer in enhancing surface properties, likely through improved protein adsorption and cell anchorage. However, the spreading remains somewhat heterogeneous.

Notably, the TiO_2 2S sample (Fig. 12c) shows the highest cell density and extensive spreading, with cells nearly covering the entire surface. The oxide layer formed by the two-step anodization likely offers a more homogeneous and stable microenvironment, promoting favorable conditions for cell adhesion and proliferation.

These observations indicate that surface modification by anodization - especially the two-step process - significantly enhances the biocompatibility of titanium, making it a promising candidate for biomedical implant applications.

After 72 hours of cell culture, SEM images further reveal a pronounced increase in both cell density and spreading across all three samples: Ti, TiO_2 1S, and TiO_2 2S (Fig. 13).

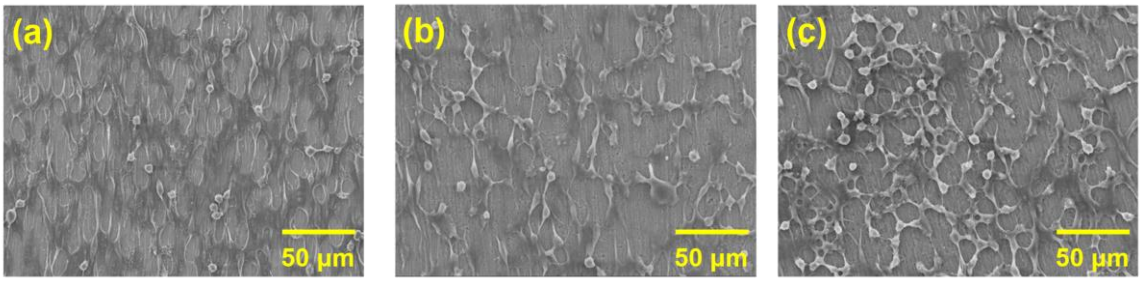

Fig. 13. SEM images showing BHK cell distribution after 72 hours of culture on (a) titanium, (b) TiO_2 1S, and (c) TiO_2 2S.

On the untreated titanium surface (Fig. 13a), although the number of cells increases compared to the 48-hour timepoint, most cells maintain an elongated morphology with limited spreading and sparse distribution. This suggests that the native titanium surface still fails to provide an optimal microenvironment for effective cell attachment and proliferation.

For the TiO_2 1S sample (Fig. 13b), cells display a more pronounced spreading behavior with extended filopodia and a tendency to form intercellular connections. The anodized surface contributes to improved biocompatibility, yet the overall surface coverage remains incomplete, indicating that the potential for full cell integration may still be limited.

The TiO_2 2S sample (Fig. 13c) shows the most outstanding performance, with high cell density, widespread flattened morphology, and extensive intercellular connections forming a continuous network across the entire surface. This outcome indicates that the oxide layer generated through the two-step anodization provides a stable and uniform surface favorable for protein adsorption and cell anchorage.

Taken together, the 72-hour results demonstrate a continued enhancement in cell adhesion and proliferation due to anodization treatment, with the TiO_2 2S sample exhibiting the most favorable surface characteristics for potential biomedical implant applications.

High-magnification SEM images after 72 hours of cell culture reveal distinct differences in the extent of cell spreading and the development of adhesion structures (filopodia) across the material surfaces (Fig. 14).

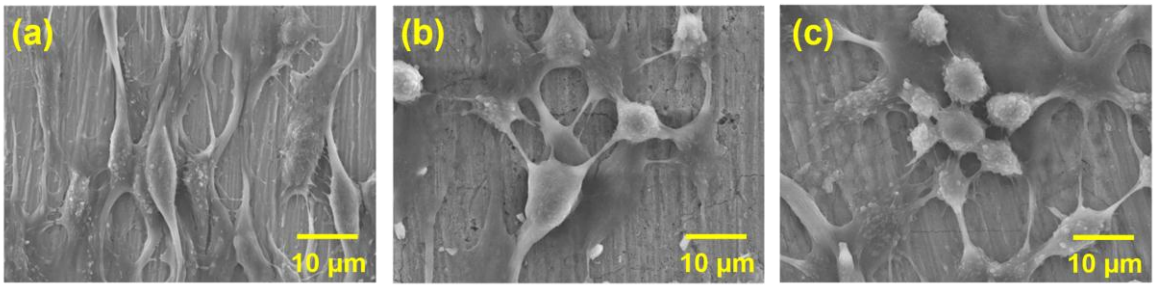

Fig. 14. SEM images of BHK cell filopodia on (a) Ti, (b) TiO_2 1S, and (c) TiO_2 2S.

On the untreated Ti sample (Fig. 14a), cells exhibit pronounced elongation along a specific direction, forming thin, extended filopodia that anchor into surface grooves. However, the number of filopodia remains limited and mainly concentrated at the two ends of the cells, indicating minimal interaction with the surface and reflecting the low bioactivity of the unmodified titanium substrate.

For the TiO_2 1S sample (Fig. 14b), cells demonstrate improved spreading with multiple filopodia projecting in various directions. Some of these extensions reach out

and attach to different surface regions, suggesting enhanced cell-material interactions due to the oxide layer formed after single-step anodization. Nevertheless, intercellular connectivity is still relatively limited.

In contrast, the TiO_2 2S sample (Fig. 14c) shows extensive cell spreading, with densely branched, elongated filopodia anchoring firmly to the substrate and interconnecting to form networks. Additionally, the presence of broad lamellipodia and densely packed adhesion points indicates strong and stable interactions between cells and the material surface. This highlights the superior support provided by the surface formed through two-step anodization in promoting cellular adhesion and environmental sensing.

Overall, the filopodia morphology observed after 72 hours further supports the conclusion that the TiO_2 oxide layer produced by two-step anodization not only enhances cell density and spreading but also stimulates the formation of adhesion structures critical for the biological integration of implant materials.

4. Conclusion

Anodization significantly enhanced the surface properties of titanium, as evidenced by distinct improvements in morphology, structural characteristics, electrochemical behavior, and biocompatibility. The two-step anodization process produced a more uniform, oxygen-rich, and stable TiO_2 oxide layer, leading to increased hardness, superior corrosion resistance (up to 52.32%), and more effective suppression of ion diffusion from the external environment.

Furthermore, the two-step anodized surface promoted superior cell adhesion and spreading, characterized by well-developed filopodia and lamellipodia, indicating strong cell-material interactions. These findings confirm the potential of two-step anodization as a promising surface treatment for biomedical implants requiring both high durability and excellent biological performance.

Acknowledgment

This research is funded by Vietnam National Foundation for Science and Technology Development (NAFOSTED) under the grant number 103.02-2023.93.

References

[1] M. Geetha, A. K. Singh, R. Asokamani, and A. K. Gogia, “Ti based biomaterials, the ultimate choice for orthopaedic implants - A review”, *Progress in Materials Science*, Vol. 54, Iss. 3, pp. 397-425, 2009. DOI: 10.1016/j.pmatsci.2008.06.004

[2] C. N. Elias, J. H. C. Lima, R. Valiev, and M. A. Meyers, “Biomedical applications of titanium and its alloys”, *Journal of Biomedical Materials Research Part B*, Vol. 87, Iss. 2, pp. 488-496, 2008. DOI: 10.1002/jbm.b.31124

[3] D. M. Brunette, P. Tengvall, M. Textor, and P. Thomsen, *Titanium in Medicine: Material Science, Surface Science, Engineering, Biological Responses and Medical Applications*, Springer, 2001.

[4] E. Szaniawska-Białas, A. Brudzisz, A. Nasir, and E. Wierzbicka, "Recent advances in preparation, modification, and application of free-standing and flow-through anodic TiO_2 nanotube membranes", *Molecules*, Vol. 29, No. 23, Nov. 2024. DOI: 10.3390/molecules29235638

[5] S. H. Oh, R. R. Finõnes, C. Daraio, L. H. Chen, and S. Jin, "Growth of nano-scale hydroxyapatite using chemically treated titanium oxide nanotubes", *Biomaterials*, Vol. 26, No. 24, pp. 4938-4943, Aug. 2005. DOI: 10.1016/j.biomaterials.2005.01.048

[6] K. C. Popat, L. E. Leoni, C. A. Grimes, and T. A. Desai, "Influence of engineered titania nanotubular surfaces on bone cells", *Biomaterials*, Vol. 28, Iss. 21, pp. 3188-3196, 2007. DOI: 10.1016/j.biomaterials.2007.03.020

[7] P. Roy, S. Berger, and P. Schmuki, "TiO_2 nanotubes: Synthesis and applications", *Angewandte Chemie International Edition*, Vol. 50, Iss. 13, pp. 2904-2939, 2011. DOI: 10.1002/anie.201001374

[8] J. M. Macák, H. Tsuchiya, A. Ghicov, and P. Schmuki, "Dye-sensitized anodic TiO_2 nanotubes", *Electrochemistry Communications*, Vol. 7, No. 11, pp. 1133-1137, 2005. DOI: 10.1016/j.elecom.2005.08.013

[9] D. Gong *et al*., "Titanium oxide nanotube arrays prepared by anodic oxidation", *Journal of Materials Research*, Vol. 16, Iss. 12, pp. 3331-3334, 2001. DOI: 10.1557/JMR.2001.0457

[10] Y. T. Sul *et al*., "Oxidized implants and their influence on the bone response", *Journal of Materials Science: Materials in Medicine*, Vol. 12, No. 10-12, pp. 1025-1031, Oct.-Dec. 2001. DOI: 10.1023/a:1012837905910

[11] H. M. Xu *et al*., "The Fabrication of highly ordered TiO_2 nanotube arrays and their application in dye-sensitized solar cells", *Advanced Materials Research*, Vols. 217-218, pp. 1553-1558, Mar. 2011. DOI: 10.4028/www.scientific.net/AMR.217-218.1553

[12] R. Narayanan, T. Y. Kwon, and K. H. Kim, "TiO_2 nanotubes from stirred glycerol/NH_4F electrolyte: Roughness, wetting behavior and adhesion for implant applications", *Materials Chemistry and Physics*, Vol. 117, Iss. 2-3, pp. 460-464, Oct. 2009. DOI: 10.1016/j.matchemphys.2009.06.023

[13] J. Azadmanjiri *et al*., "Enhanced attachment of human mesenchymal stem cells on nanograined titania surfaces", *RSC Advances*, Vol. 6, No. 61, 2016. DOI: 10.1039/C6RA10289A

[14] Y. Zhang *et al*., "Mineralization and osteoblast behavior of multilayered films on TiO_2 nanotube surfaces assembled by the layer-by-layer technique", *Chinese Chemical Letters*, Vol. 27, No. 7, pp. 1091-1096, 2016. DOI: 10.1016/j.cclet.2016.03.035

[15] P. Roy, D. Kim, K. Lee, and E. Spiecker, "TiO_2 nanotubes and their application in dye-sensitized solar cells", *Nanoscale*, Vol. 2, No. 1, pp. 45-59, 2010. DOI: 10.1039/b9nr00131j

[16] K. Lee, A. Mazare, and P. Schmuki, "One-dimensional titanium dioxide nanomaterials: Nanotubes", *Chemical Reviews*, Vol. 114, Iss. 19, pp. 9385-9454, 2014. DOI: 10.1021/cr500061m

[17] X. Wang *et al.*, "Review of water-assisted crystallization for TiO_2 nanotubes", *Nano-Micro Letters*, Vol. 10, Art. 77, 2018. DOI: 10.1007/s40820-018-0230-4

[18] D. Prando, A. Brenna, F. M. Bolzoni, and M. V. Diamanti, "Electrochemical anodizing treatment to enhance localized corrosion resistance of pure titanium", *Journal of Applied Biomaterials & Functional Materials*, Vol. 15, Iss. 1, 2017. DOI: 10.5301/jabfm.5000344

[19] J. Quinn, R. McFadden, C. W. Chan, and L. Carson, "Titanium for orthopedic applications: An overview of surface modification to improve biocompatibility and prevent bacterial biofilm formation", *iScience*, Vol. 23, Iss. 11, 2020. DOI: 10.1016/j.isci.2020.101745

[20] Q. Yu *et al.*, "Fabrication of TiO_2 nanotube arrays by a two-step anodic oxidation", *Rare Metal Materials and Engineering*, Vol. 40, pp. 201-205, July 2011.

[21] J. W. Nicholson, "Titanium alloys for dental implants: A review", *Prosthesis*, Vol. 2, Iss. 2, pp. 100-116, 2020. DOI: 10.3390/prosthesis2020011

[22] C. C. Chiang, J. S. Li, H. H. Wan, F. Ren, J. F. Esquivel-Upshaw, "Fabrication of TiO_2 nanotube arrays by progressive anodization of Ti thin film on insulated substrates", *Materials*, Vol. 18, No. 6, Mar. 2025. DOI: 10.3390/ma18061219

[23] JCPDS, "Titanium (PDF 44-1294)", *Powder Diffraction File*, Joint Committee on Powder Diffraction Standards - International Centre for Diffraction Data, 1996.

[24] A. Sandoval-Amador *et al.*, "Influence of anodization conditions in hydrofluoric acid electrolyte on the optimization of TiO_2 nanotube surfaces", *Applied Physics A: Materials Science & Processing*, Vol. 131, p. 609, July 2025. DOI: 10.1007/s00339-025-08743-0

[25] R. A. Ocampo and F. E. Echeverría, "The effects of anodization conditions on TiO_2 nanotubes features obtained using aqueous electrolytes with xanthan gum", *Inventions*, Vol. 8, No. 5, Aug. 2023. DOI: 10.3390/inventions8050109

[26] JCPDS, "Titanium dioxide (anatase) (PDF 21-1272)", *Powder Diffraction File*, Joint Committee on Powder Diffraction Standards - International Centre for Diffraction Data, 1996.

[27] JCPDS, "Titanium dioxide (rutile) (PDF 21-1276)", *Powder Diffraction File*, Joint Committee on Powder Diffraction Standards - International Centre for Diffraction Data, 1996.

[28] B. Wu, Y. Tang, K. Wang, X. Zhou, and L. Xiang, "Nanostructured titanium implant surface facilitating osseointegration from protein adsorption to osteogenesis: the example of TiO_2 NTAs", *International Journal of Nanomedicine*, Vol. 17, pp. 1865-1879, Apr. 2022. DOI: 10.2147/IJN.S362720

[29] T. M. David, P. R. Dev, P. Wilson, P. Sagayaraj, and T. Mathews, "A critical review on the variations in anodization parameters toward microstructural formation of TiO_2 nanotubes", *Electrochemical Science Advances*, Vol. 1, No. 8, Aug. 2021. DOI: 10.1002/elsa.202100083

[30] A. Jędrzejewska and K. Arkusz, "Mechanism and growth kinetics of hexagonal TiO_2 nanotubes with an influence of anodizing parameters on morphology and physical properties", *Scientific Reports*, Vol. 14, p. 24721, 2024. DOI: 10.1038/s41598-024-76336-7

PHÂN TÍCH SO SÁNH LỚP ỐNG NANO TiO_2 HÌNH THÀNH BẰNG PHƯƠNG PHÁP ANỐT HÓA MỘT BƯỚC VÀ HAI BƯỚC: HÌNH THÁI BỀ MẶT, KHẢ NĂNG CHỐNG ĂN MÒN VÀ ĐÁP ỨNG TẾ BÀO

Lê Văn Toán[1,2], Đặng Minh Đức[1], Vũ Công Mạnh[1], Phạm Hùng Vượng[1,3]

[1]*Trường Vật liệu, Đại học Bách khoa Hà Nội*

[2]*Khoa Hóa - Lý kỹ thuật, Trường Đại học Kỹ thuật Lê Quý Đôn*

[3]*Phòng Thí nghiệm Vật liệu Y sinh, Đại học Bách khoa Hà Nội*

Tóm tắt: Nghiên cứu này đánh giá ảnh hưởng của các quy trình anốt hóa đến sự hình thành và đặc tính của lớp ống nano TiO_2 trên titan thương mại tinh khiết (cp-Ti) ứng dụng trong cấy ghép y sinh. Cả anốt hóa một bước (TiO_2 1S) và hai bước (TiO_2 2S) đều tạo ra cấu trúc ống nano gồm hai pha anatase và rutile, trong đó phương pháp hai bước cho thấy các ống nano đồng đều và sắp xếp thẳng đứng hơn. Thử nghiệm cơ học cho thấy độ cứng bề mặt tăng lên, trong khi phân tích điện hóa chứng minh khả năng chống ăn mòn được cải thiện, đặc biệt ở mẫu TiO_2 2S. Ngoài ra, bề mặt TiO_2 2S còn thúc đẩy sự bám dính và lan tỏa tế bào tốt hơn, với các cấu trúc filopodia và lamellipodia phát triển rõ rệt. Nhìn chung, anốt hóa hai bước tạo ra lớp oxit giàu oxy ổn định hơn với độ bền và khả năng tương thích sinh học vượt trội, cho thấy tiềm năng ứng dụng trong các vật liệu cấy ghép xương.

Từ khóa: *Titan; ống nano TiO_2; anốt hóa; biến tính bề mặt; chống ăn mòn; bám dính tế bào; cấy ghép y sinh.*

Received: 16/07/2025; Revised: 20/09/2025; Accepted for publication: 29/10/2025

❑